Slow manifold structure and the emergence of mixed-mode oscillations

Andrei Goryachev
Chemical Physics Theory Group, Department of Chemistry, University of Toronto, Toronto, ON M5S 3H6, Canada

Peter Strizhak
L.V. Pisarzhevskii Institute of Physical Chemistry, Ukrainian Academy of Sciences, p. Nauki 31, Kiev, Ukraine, 25203

Raymond Kapral
Chemical Physics Theory Group, Department of Chemistry, University of Toronto, Toronto, ON M5S 3H6, Canada

A detailed study of the slow manifold of a model exhibiting mixed-mode oscillations is presented. A scenario for the emergence of mixed-mode states which does not involve phase locking on a 2-torus is constructed. We show that mixed-modes correspond to the periodic orbits embedded in the horseshoe-type strange set and demonstrate how transformations of this set determine the transitions of mixed-mode states into each other. © *1997 American Institute of Physics.* [S0021-9606(97)51931-3]

I. INTRODUCTION

Oscillatory behavior exhibited by nonlinear chemical systems often takes the form of periodic mixed-mode oscillations consisting of L large amplitude oscillations followed by S small amplitude oscillations. The distinctive difference between large and small oscillations allows one to classify the mixed-mode oscillatory states by integer pairs (L,S) and assign them the symbol L^S. Ordered progressions of such periodic patterns separated by chaotic oscillations are observed as control parameters are varied. The progressions of different mixed-mode forms are known to be Farey sequences described by Farey arithmetic.[1]

Since their discovery in the Belousov–Zhabotinsky reaction,[2] mixed-mode oscillations have been found in a broad range of chemical and biological[3] systems. Their ubiquity suggests the possibility of the existence of a common dynamical systems theory origin. A number of authors[1,4] identified experimentally observed mixed-mode oscillations with periodic motions arising as a result of phase-locking on a 2-torus. This hypothesis was based mainly on the fact that the periodic states on an invariant torus form Farey sequences as a control parameter runs through the quasiperiodic route from period-1 oscillations to chaos. Numerical evidence for the existence of quasiperiodicity and torus oscillations was obtained from studies of model systems which exhibit mixed-mode oscillations.[5,6]

However, there are results which show that mixed-mode oscillations cannot be attributed to the phenomenon of quasiperiodicity in all systems. In a study of electrodissolution of copper Albahadily *et al.*[7] demonstrated that the mixed-mode states emerge in parameter regions different from those where a torus is stable. The formation of mixed-mode oscillations was observed at a point well beyond the range of parameters between the secondary Hopf bifurcation and the torus break-up bifurcation, where the mixed-mode states should lie according to the hypothesis of quasiperiodicity. In a series of electrochemical studies Koper *et al.*[8] found that the mixed-mode oscillations in Farey sequences observed in their study are separated by chaotic states which resemble random mixtures of the adjacent periodic patterns rather than by quasiperiodic oscillations densely covering the surface of a 2-torus. In a numerical study of a model system Koper[9] found a parameter domain where both quasiperiodic oscillations lying on a 2-torus and a large-amplitude mixed-mode oscillatory state which does not belong to the torus are stable simultaneously. In order to interpret the results of the experimental study in Ref. 7 Ringland *et al.*[10] constructed a family of two-extremum Z-maps capable of producing Farey sequences in the limiting case when the central segment of the Z-map is vertical. They have shown that one may obtain Farey sequences which are not related to phase locking on a torus.

In this paper we present results of investigations of a model proposed earlier for the qualitative description of the mixed-mode oscillations observed in the Belousov–Zhabotinsky reaction.[11] From the analysis of the transformation of the slow manifold of the model as system parameters are changed we demonstrate the gradual emergence of a horseshoe-type strange set in which all the mixed-mode states are embedded as periodic orbits. On the basis of this analysis we construct a three-dimensional phase space picture describing the emergence and bifurcations of mixed-mode states. This scenario does not involve a torus and appears to be an alternative to the well-established quasiperiodic scenario.

In Sec. II we introduce the model and present a brief discussion of its attractors and bifurcation structure. Section III is devoted to the detailed analysis of the slow manifold and a description of its important properties. We introduce a technique that allows us to construct the slow manifold and demonstrate how it turns into a horseshoe by stretching and folding. The repulsive flow that defines a particular shape of mixed-mode oscillations is introduced and discussed in some

detail. In Sec. IV we show that when the slow manifold is folded into a horseshoe interacting with the repulsive flow, the mixed-mode oscillations arise naturally at the point where the large-amplitude, period-1 oscillation loses its stability through a saddle-node bifurcation. The relation of the phase flow on the horseshoe to the Z-map introduced by Ringland et al.[10] is discussed. In Sec. V we conclude that the existence of the repulsive flow allows one to consider this horseshoe as a representative of a distinct subclass of strange sets whose periodic windows are organized according to Farey sequences.

II. DESCRIPTION OF THE MODEL

We consider a three-variable extension[12] of the Boissonade–De Kepper model,[13]

$$\dot{x} = \gamma(y - x^3 + 3\mu x),$$

$$\dot{y} = -2\mu x - y - z + \beta, \tag{1}$$

$$\dot{z} = \kappa(x - z).$$

System (1) was originally proposed in Ref. 11 in order to obtain a qualitative description of transient mixed-mode oscillations in the Belousov–Zhabotinsky reaction. Depending on the values of μ and β, system (1) possesses either one or three steady states. The change in the number of stationary points occurs on the curve

$$\left(\frac{\beta}{2}\right)^2 = \left(\frac{\mu - 1}{3}\right)^3, \tag{2}$$

where two steady states coalesce or emerge in a saddle-node bifurcation. At $\mu = 1$, $\beta = 0$, where two branches of curve (2) meet in a cusp point, the pitch-fork bifurcation takes place. Note that the parameters γ and κ only rescale the corresponding components of the vector field and do not influence the positions of the nullclines and steady states in phase space. In the following discussion the geometric parameters μ and β are fixed ($\mu = 2.0$, $\beta = -0.4$) while γ and κ are varied. With this choice of μ and β system (1) has only one steady state at $x_f = z_f = -1.159705$, $y_f = 5.398524$, which is a stable focus in a domain of the parameter plane (γ, κ) lying to the left of the Hopf bifurcation line (see Fig. 1), and a saddle-focus otherwise. As the real characteristic exponent of the steady state is negative everywhere on (γ, κ), no second order bifurcation is possible at the chosen values of μ and β.

Figure 1 shows the partition of the (γ, κ) plane into domains of different types of dynamical behavior according to the results of numerical integration. In domain 1 a stable focus is the only attractor of the system (1). Large amplitude period-1 (1^0) oscillations with a strong relaxational character at large γ are found in domain 2. Finally, mixed-mode oscillations are observed in the wedge-shaped domain 3. Transitions from period-1 to mixed-modes take place on an almost flat curve (shown by the dashed line in Fig. 1) where the trajectory of system (1) performs a small-amplitude excursion only once on the entire time interval t
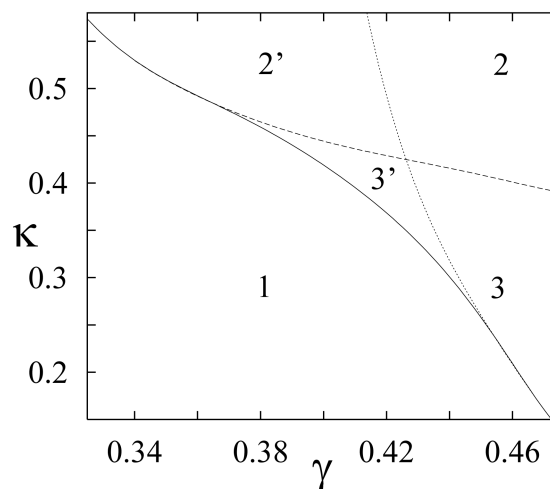
FIG. 1. Bifurcation phase diagram: 1 — steady state (focus), 2 — period-1, 3 — mixed-mode oscillations. Separating lines correspond to the Hopf bifurcation (dots), transition $1^0 \leftrightarrow \infty^1$ (dashes), and crash onto the focus (solid). Both steady state and oscillations are stable in subdomains 2' and 3'.

$\in (-\infty, +\infty)$. This transition can be represented symbolically as $1^0 \leftrightarrow \infty^1$. Continuing to traverse domain 3 by decreasing γ at constant κ one observes pruned Farey sequences of periodic mixed-mode oscillations $\infty^1 \to n^1 \to 1^1 \to 1^n \to 1^\infty$ interspersed by narrow, yet detectable, spans of chaos. This periodic-chaotic progression ends suddenly in a crash onto the focus at the point where the line separating zones 1 and 3 is crossed. At large κ ($\kappa \gtrsim 0.54$), where the crash bifurcation curve appears to be tangential to that for the $1^0 \leftrightarrow \infty^1$ transition, both bifurcations occur within an extremely narrow parameter span and one observes hard termination/emergence of large-amplitude periodic oscillations. Another limiting case is observed at low κ ($\kappa \lesssim 0.20$) where the crash curve merges with the Hopf bifurcation line. Here the crash occurs from pattern $1^n, n \gg 1$ which forms an almost homoclinic connection to the focus undergoing the Hopf bifurcation.

As κ varies the appearance of the phase portrait of the mixed-mode states changes considerably. At large values of κ both small- and large-amplitude excursions lie almost on the same plane. This type of mixed-mode oscillation, referred to as type-1 according to classification given in Ref. 8, is shown in Figs. 2(a) and 2(b). With a decrease in κ the reinjection part of trajectory falls closer to the focus and the angle between the planes of small- and large-amplitude oscillations grows. At $\kappa \lesssim 0.2$ the phase portrait of the oscillation acquires all of the features characteristic of type-2 mixed-mode states. Here the large loops are mainly orthogonal to the small ones and the reinjection occurs along the one-dimensional stable manifold of the focus [see Figs. 2(c) and 2(d)].

III. CONSTRUCTION OF THE PHASE FLOW

The parameter region in which complex periodic and chaotic oscillations are found can be partitioned into subdomains corresponding to particular periodic mixed-mode states L^S and their chaotic mixtures. We shall study the
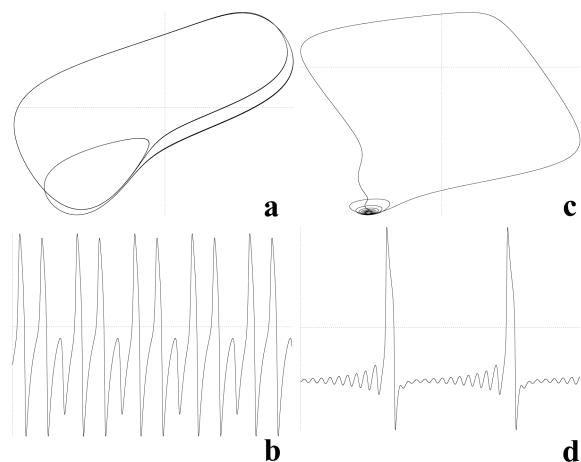
FIG. 2. Projections of the phase portraits on (x,z) plane and corresponding $x(t)$ time series for two periodic mixed-mode states: (a,b) — 2^1 for $\kappa=0.5, \gamma=0.35516$; (c,d) — 1^{12} for $\kappa=0.2, \gamma=0.471$.

mechanisms responsible for the bifurcations of one mixed-mode state into another by analyzing transformations of the phase flow on the system's slow manifold.

The concept of a slow manifold relies on the assumption that the relaxation of an arbitrary initial condition to the attractor has two characteristic time scales: the trajectory quickly reaches certain subset of the phase space and then slowly approaches the attractor within this subset. In the case of a strongly dissipative system with three dynamical variables, the slow set is usually represented by a 2D manifold which is often folded in the 3D phase space. To avoid complications arising from nontrivial embedding of the slow manifold, we choose for its construction the region of large κ where the slow manifold appears to have a relatively simple organization.

A. Slow manifold

Figure 3(a) presents the projection of the phase flow on the (x,y) plane for $\kappa=0.55$ and $\gamma=0.39$. For these parameter values deep within domain $2'$ system (1) is bistable. Apart from the stable focus, two stationary periodic solutions exist: a stable, large-amplitude, period-1 limit cycle (solid line) and a saddle-type, small-amplitude cycle (dashed line). The planar, concentric organization of these cycles around the focus suggests that the slow manifold containing them is flat. Trajectories that leave the saddle cycle at $t \to -\infty$ and approach stable cycle or focus at $t \to +\infty$ lie in the slow manifold. These trajectories are easy to calculate and one can use them for the construction of a Poincaré section of the slow manifold. We choose $P=\{x=x_f, y<y_f\}$ shown in Figs. 3(a) and 3(b) as a surface of section. Intersections of the transient trajectories with P yield a set of points which, after interpolation by a smooth function $z=z(y)$,[14] becomes a continuous zero-order approximation $A_0=\{x=x_f, y<y_f, z=z(y)\}$ to the Poincaré section of the slow manifold.

Figure 3(b) shows a 3D phase portrait of the same trajectories as in Fig. 3(a), as well as P and A_0. The intersections of the flow initiated on A_0 with P can be used both to
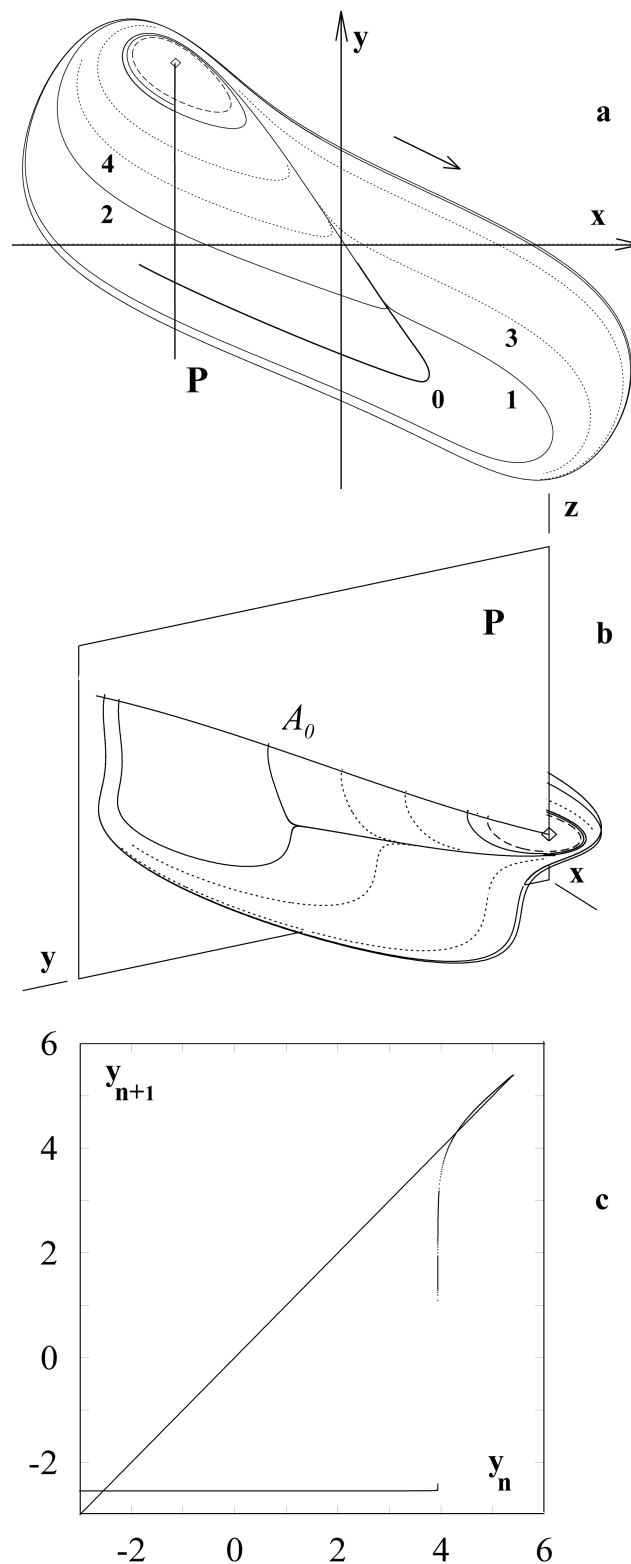
FIG. 3. Phase flow on the slow manifold. (a) Projection of the flow on (x,y) plane. (b) Mutual positions of the slow manifold and the surface-of-section P in phase space. (c) First return map for the flow initiated on A_0.

improve the accuracy of the approximation and to construct the first return map [see Fig. 3(c)] which quantitatively describes the phase flow on the slow manifold.

A complete description of the phase flow on the slow
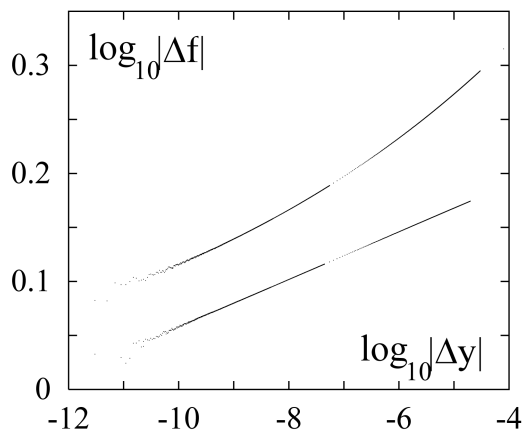
FIG. 4. Scaling of $f(y)$ at the point y_0 where tangent is vertical.

manifold can be obtained from the comparison of the phase portrait and the first return map. Consider the example presented in Figs. 3(a) and 3(c). The first return map $y_{n+1} = f(y_n)$ intersects the bisectrix in three points which correspond to the stable limit cycle ($y_c = -2.5437$), the saddle cycle ($y_s = 4.2998$), and the stable focus ($y_f = 5.3985$). The nearly rectangular shape of the map implies that the slow manifold comprises areas of strong expansion (the neighborhood of $y_0 = 3.9370$, where the map is vertical) and contraction (horizontal part of the map). In the course of its evolution a trajectory initiated in the vicinity of the saddle cycle executes a number of small-amplitude loops around the saddle cycle and then in one turn reaches the neighborhood of the stable limit cycle. Whether the trajectory approaches the limit cycle like trajectory 3 performing small transient loop or like trajectory 4 which makes a large loop depends on its position relative to a certain boundary trajectory 0 which can be identified with the point y_0 on the first return map where $f(y)$ has a vertical tangent. Analysis of $f(y)$ in a small neighborhood of y_0 shows that the trajectory 0 is superunstable; i.e., the neighboring trajectories deviate from it faster than geometrically. Figure 4 shows $\log_{10}|\Delta f|$ versus $\log_{10}|\Delta y|$, where $\Delta f = f(y) - f(y_0)$ and $\Delta y = y - y_0$, for both left $y < y_0$ (lower set of points) and right $y > y_0$ (upper set) branches of the map shown in Fig. 3(c). One can see that for Δy sufficiently small, $\Delta f(\Delta y)$ is characterized by the power law $\Delta f \propto (\Delta y)^\alpha$ where $\alpha \approx 0.022 \ll 1$. This implies an extreme divergence of trajectories which is also reflected in the phase portrait. The initial conditions $(x_f, y_1, z(y_1)), (x_f, y_2, z(y_2))$ on P for trajectories 1 and 2 [solid lines in Figs. 3(a) and 3(b)] were such that $y_1 = y_0 - \delta/2$, $y_2 = y_0 + \delta/2$ where $\delta = 10^{-12}$. As Fig. 3 shows, the separation between these two trajectories on their return to the surface of section grows by ≈ 12 orders of magnitude. In fact, trajectories 3 and 4 constitute another pair with $\delta = 10^{-10}$.

The existence of the superunstable trajectory results in the observed dichotomy of trajectories belonging to the slow manifold. A 2D manifold intersecting the slow manifold along trajectory 0 plays similar separating role in the 3D phase space. Although the global structure of this repulsive

flow in the phase space is very complicated, the flow can be easily determined locally by the property that it separates trajectories making large and small loops while approaching the attractor.

B. Birth of the horseshoe

Figure 5(a) shows an expanded view of the flat part of the first return map $f(y)$ in Fig. 3(c). The slope of the map is everywhere positive and, thus, the map is invertible. As γ decreases at constant $\kappa = 0.55$, a smooth transformation of the slow manifold takes place, resulting in the loss of invertability of the map. A fragment of map constructed for $\gamma = 0.332241$ [see Fig. 5(b)] demonstrates that $f(y)$ is not monotonic and a smooth maximum arises near the stable limit cycle. At $\gamma = 0.33224025$ the map is tangent to the bisectrix and a new pair of stable and unstable limit cycles emerges on the slow manifold [cf. Fig. 5(c)]. As the map's maximum grows it sharpens and the newborn limit cycle loses its stability through a cascade of period-doubling bifurcations. At $\gamma = 0.3322392$ [see Fig. 5(d)] a chaotic attractor coexists with the period-1 limit cycle and focus. Although the entire cascade to chaos occupies very narrow span of γ, two first period-doubling bifurcations were resolved. The tristability of the system breaks down at a certain value of γ and every trajectory initiated near the maximum of the map is attracted to the period-1 limit cycle after a chaotic transient of varying length.

Figure 5(e) shows a part of the first return map for $\gamma_c = 0.332239127$ where oscillations suddenly crash on the focus. Two important characteristic features of the flow can be inferred from the map. First, the maximum of the map acquires a cuspoid shape signaling of the formation of a highly compressed fold on the slow manifold. Second, from the tangency of the map and bisectrix, one can see that the stable period-1 limit cycle and the large-amplitude saddle cycle are near the point of coalescence. The annihilation of this pair in a saddle-node bifurcation gives rise to an intermittent chaotic attractor which has the appearance of a thick limit cycle. A decrease in the control parameter γ leads to the crash of chaotic oscillations onto the focus. Summarizing the information presented in Figs. 5(a)–5(e), one can conclude that as γ changes through the interval $[0.39, \gamma_c]$, the slow manifold transforms from a planar surface into a folded fractal structure with infinitely many leaves (Smale's horseshoe).

Making use of several auxiliary Poincaré sections it is possible to construct a 3D picture of the slow manifold. Figure 6 schematically represents the manifold and three of its Poincaré sections at parameters close to the crash bifurcation. Part of the manifold situated between sections C and A is removed to facilitate visualization of its geometry. In section A one sees a triply-folded curve which corresponds to the first structural level of the manifold. Note the difference between the two folds of this curve: while the outer fold has a smooth parabolic shape, the inner fold is a sharp cusp. Increasing the resolution considerably (by ≈ 5 orders of magnitude) one would be able to find that the curve is, in
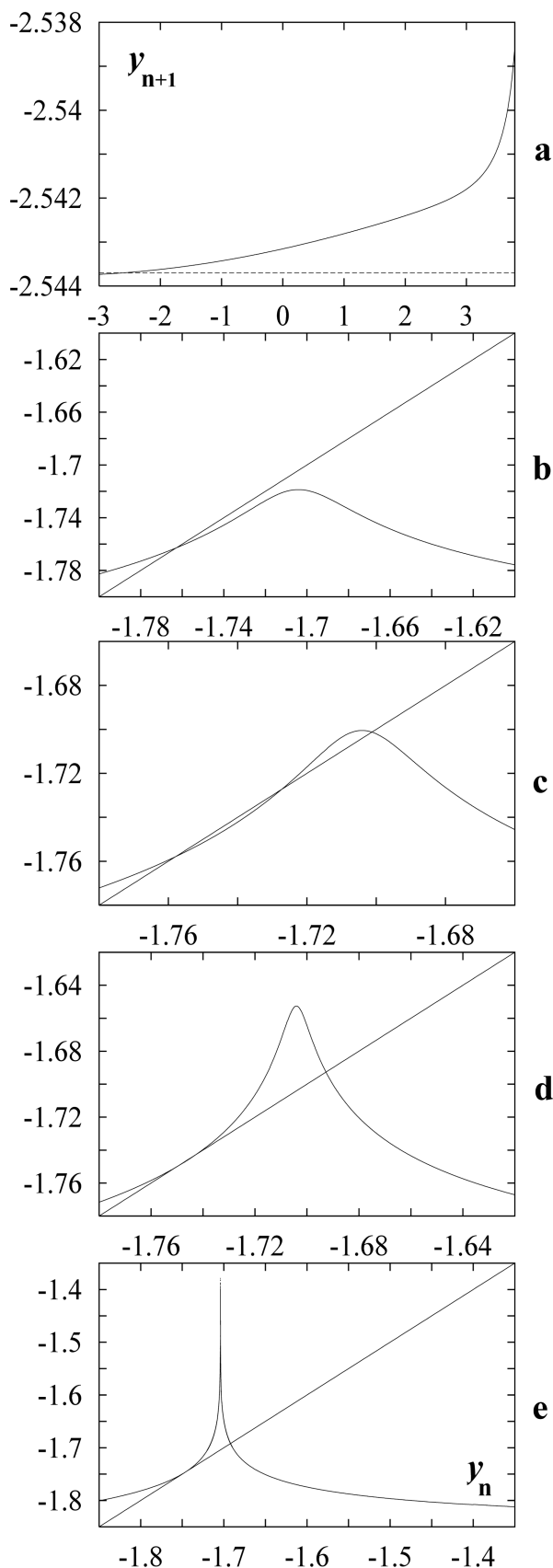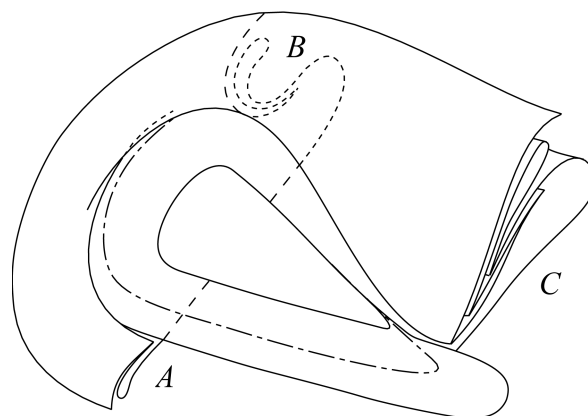
FIG. 6. Geometry of the folded slow manifold. The superunstable trajectory is shown by dot-and-dash line.

fact, a densely compressed fold constituted by seven leaves of the second structural level, and so on. To describe one iteration of the manifold stretching and folding we do not need to consider these higher structural levels. Following the evolution of points in section A under the flow (clockwise in Fig. 6) one encounters a pleat where the manifold as a whole begins to fold into an S-shaped form (section B) with two approximately equal parabolic folds. Prominent stretching of the flow in the plane of the manifold, accompanied by strong contraction in the orthogonal direction, transforms the manifold into the thin roll composed of seven leaves seen in section C. As a result of the extreme inhomogeneity of compression the inner fold acquires sharp cuspoid shape while the outer one remains smooth and parabolic. As the flow returns to section A more contraction along the vertical direction occurs and the second order structure shown in section C is not discernible.

IV. MIXED-MODE OSCILLATIONS

In Sec. III we described two important characteristic features of the phase flow of system (1). Firstly, at the parameter values in the neighborhood of mixed-mode oscillations, the slow manifold is folded into a horseshoe-type set with a fractal, multi-leaved structure. Secondly, the repulsive flow divides the transient trajectories into two distinct classes. Intersection of the repulsive flow and the slow manifold yields a superunstable trajectory with peculiar dynamical properties. In the present section we show how mixed-mode states which correspond to periodic orbits embedded in the horseshoe emerge and bifurcate into each other.

A. Emergence of mixed-mode oscillations

Consider a path in the (γ, κ) parameter plane which starts in domain 2 or $2'$ and ends in the region of mixed-mode oscillations 3 (see Fig. 1). As the domain of large-amplitude period-1 oscillations is traversed towards the curve corresponding to the $1^0 \leftrightarrow \infty^1$ transition, the modifications of the slow manifold described in Sec. III B take place. Before the first mixed-mode is formed an important transformation of the manifold occurs at the point where a cusp-

FIG. 5. Transformation of the first return map at $\kappa = 0.55$ and decreasing γ: (a) $\gamma = 0.39$, (b) $\gamma = 0.332241$, (c) $\gamma = 0.3322399$, (d) $\gamma = 0.3322392$, (e) $\gamma = 0.332239127$.
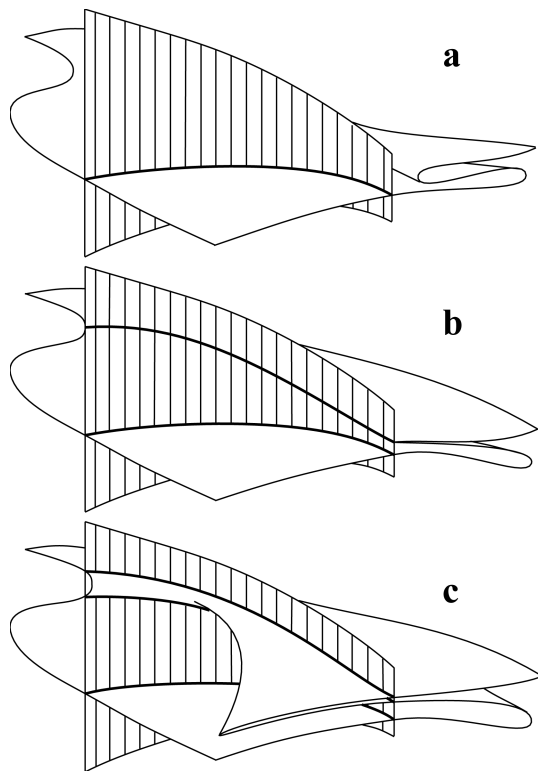
FIG. 7. Propagation of the slow manifold through the surface of the repulsive flow (hatched): (a) $\gamma > \gamma_c$ — transversal intersection; (b) $\gamma = \gamma_c$ — formation of a tangency; (c) $\gamma < \gamma_c$ — fold penetrates the surface.

FIG. 8. First return map at the point of the $1^0 \leftrightarrow \infty^1$ transition ($\kappa = 0.5$, $\gamma = 0.355403274$).

shaped fold develops. Inspection of Fig. 6 shows that the manifold cannot support periodic oscillations with small-amplitude loops since its folded part lies on the ''large-amplitude'' side of the repulsive flow (only the superunstable trajectory is shown in Fig. 6). In order for orbits with both small- and large-amplitude excursions to exist, the repulsive flow has to intersect the folded part of the horseshoe.

Figure 7 shows segments of the manifolds cut out by two orthogonal planes for three consecutive values of γ and fixed κ. The case $\gamma > \gamma_c$ [Fig. 7(a)] corresponds to the generic transversal position of the manifolds in which the growing fold of the horseshoe lies on one side of the repulsive flow. This case is described by a first return map of the type shown in Fig. 5(d). At $\gamma = \gamma_c$, in addition to the transversal intersection, a tangency between the two manifolds occurs. The tangency manifests itself by the formation of a sharp cusp on the first return map [see Fig. 5(e)]. For $\gamma < \gamma_c$ the fold of the horseshoe penetrates the surface corresponding to the repulsive flow and drastically increases in size due to the strong divergence from the repulsive flow. One also sees in Fig. 7(c) that as a result of this transformation two new superunstable orbits (thick solid lines) are born on the slow manifold. Taking into consideration the fractal nature of the horseshoe one could imagine an infinite stack of superunstable orbits born in pairs when nested folds of the horseshoe penetrate the surface of the repulsive flow one by one.

The birth of new superunstable orbits is reflected in the first return map as well. Figure 8 shows the first return map constructed with P as a surface of section as described in

Sec. III A for parameter values $\kappa = 0.50$, $\gamma_0 = 0.355403274 < \gamma_c$ at which the transition $1^0 \leftrightarrow \infty^1$ occurs. As γ_c is passed, the cusp on the map breaks up and the maximum acquires normal parabolic shape. At the same time the height of the maximum increases tremendously and two segments with infinite slope appear on its sides.

The analysis of the map shows that the transition $1^0 \leftrightarrow \infty^1$ occurs simultaneously with annihilation of the large-amplitude stable and saddle-type limit cycles. At the point of coalescence they produce structurally unstable limit cycle which is seen on the first return map as a point of tangency with bisectrix. This cycle combines properties of both stable and unstable limit cycles. Consider a trajectory which departs from such cycle at $t \to -\infty$. In the course of evolution it inevitably executes one small-amplitude loop around the focus. Upon the completion of this loop the trajectory is reinjected into the stable part of the neighborhood of the cycle which is eventually approached at $t \to +\infty$. Thus, first mixed-mode state ∞^1 is characterized by the orbit homoclinic to the structurally unstable cycle and, therefore, exists in a parameter domain of zero measure. For $\gamma < \gamma_0$ a finite number of large-amplitude loops is executed before a trajectory visits the small loop and successions of n^1 mixed-mode states with rapidly decreasing n are observed.

B. Embedding of the mixed-mode orbits

It is possible to establish how a particular mixed-mode orbit is incorporated in the slow manifold. Figure 9 shows the (x, y) projection of a 46^1 orbit and its embedding in the horseshoe. As in Fig. 6, the Poincaré sections of the manifold are shown at different levels of resolution of the fine structure. While section A presents the first two structural levels, in section B only first level is shown in full. Two lines of phase points parallel to the surface of the repulsive flow and separated from it by $\delta = \pm 0.5 \times 10^{-12}$ are selected in section A (long dashes). The evolution of these points shown in section B demonstrates the extreme divergence of trajectories caused by the presence of the repulsive flow.
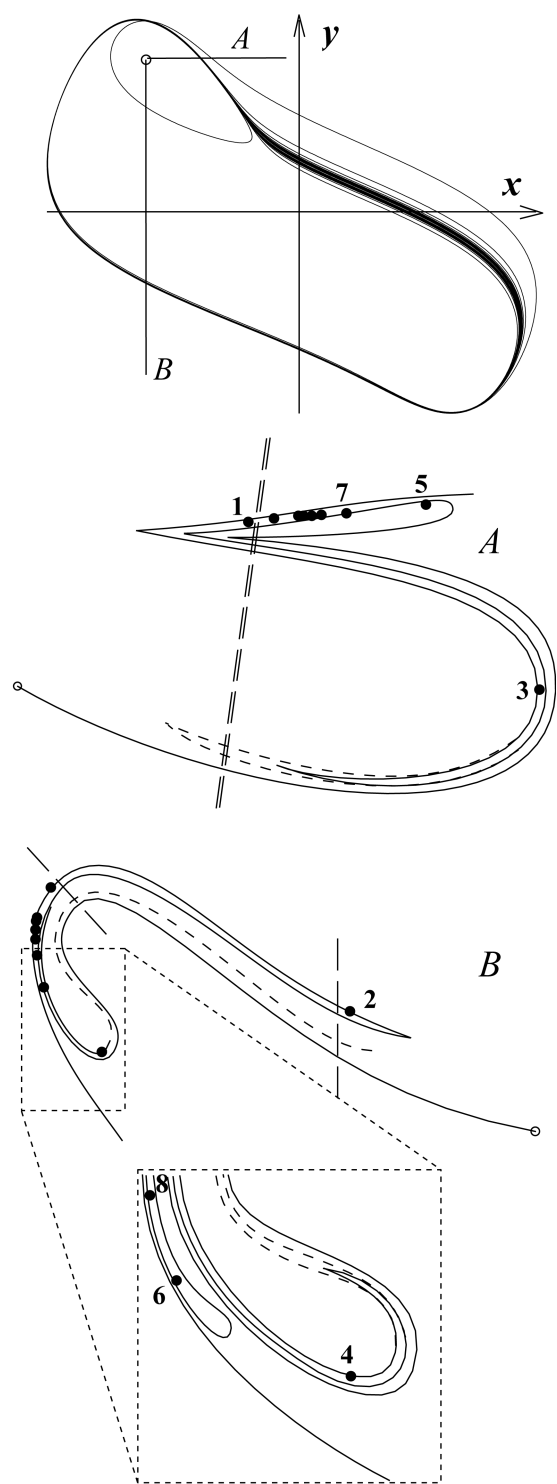
FIG. 9. Projection of 46^1 orbit onto (x,y) plane and its embedding in the slow manifold (see discussion in the text).

Orbit 46^1 consists of a dense, flat band of large-amplitude loops which consecutively shrink in size and a small loop where the trajectory segment is reinjected into the large-amplitude band. Projecting points in which the orbit intersects planes A and B (shown by thick dots) on the corresponding Poincaré sections of the horseshoe one can obtain insight into the mechanism of this reinjection. At a certain

time the trajectory appears to the left of the repulsive flow surface (point 1 in A). This causes it to execute a small loop (point 2 on the cusp-shaped tongue in B). Next return of the trajectory into section A occurs in point 3, separated far from 1. Following the subsequent numbers one sees how the orbit returns to the large-amplitude band, gradually ascending leaves of the slow manifold. The same mechanism holds for all $\mathbf{n}^1$ states, although escape on the small loop occurs from different leaves.

The analysis of the reinjection scheme shows that the horseshoe (solid lines in Fig. 9) cannot support mixed-mode oscillations with more than one small-amplitude loop. Indeed, regardless of how far to the left one shifts the position of point 1, first return of a trajectory initiated at 1 into the surface of section (point 3) lies to the right of the repulsive flow. This situation changes as the cusp-shaped tongue, to which point 3 belongs, penetrates the surface of the repulsive flow through the formation of a tangency as described in Sec. IV A. (Corresponding changes on both sections are shown by medium-dashed lines.) As soon as a similar tongue of a higher structural level passes through the surface of the repulsive flow, an opportunity for the existence of the third small-amplitude loop arises, and so on. Thus, changing position of the horseshoe relative to the repulsive flow one can obtain mixed-mode states L^S with any desired L and S.

C. Relation to Z-map

At small values of κ, where the bulk of the mixed-mode domain lies, the surface-of-section P introduced in Sec. III A becomes unsuitable for the construction of the first return map due to the strongly bent shape of the corresponding Poincaré section (see section B in Fig. 9). Instead, one can use sections $y =$ const similar to section A in Fig. 9. Figure 10 presents two examples of the first return map $x_{n+1} = f_Z(x_n)$ constructed in the approximation based on the upper leaf of the horseshoe for parameter values corresponding to 46^1 (a) and 1^1 (b) mixed-mode states.

As one can see, maps of this type share a number of common features. The map consists of two branches with positive slope and an extremely steep, negatively-inclined segment which joins the branches. At the point corresponding to the superunstable orbit the map has an infinite slope and can be locally described by an exponent as discussed in Sec. III A. Any mixed-mode state L^S may be represented on this map by a periodic trajectory with L iterates on the right branch and S iterates on the left branch. This property of the map makes it particularly suitable for the illustration of mixed-mode bifurcations. At parameter values corresponding to the transition $1^0 \leftrightarrow \infty^1$ the right branch is tangent to the bisectrix. As an intermittent channel opens, the trajectory funnels through it and then jumps onto the left branch from which it is reinjected onto the branch of large-amplitude loops and the cycle closes. As γ decreases both branches fall relative to the bisectrix, reflecting the gradual growth of the number of small-amplitude loops accompanied by a reduction in the number of large-amplitude loops.

In Ref. 10 Ringland *et al.* extensively studied the prop-
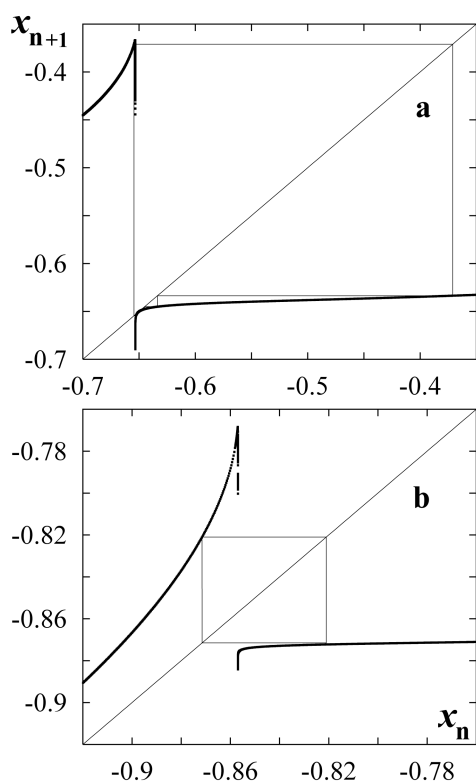
FIG. 10. First return maps $f_Z(x)$ constructed for $\kappa=0.4$ with $y=0.4$ as a surface-of-section: (a) $\gamma=0.46204$, (b) $\gamma=0.44$. Orbits 46^1 and 1^1 are shown with thin solid lines.

erties of the two-extremum map $x_{n+1}=Z(x_n)$ where

$$Z(x)=(c+ax)(1-\tanh(sx))+(d+bx)(1+\tanh(sx)).$$

At small values of the parameter s the map has a smooth shape similar to that of the cubic map. As s increases, the slope of its middle, negatively-inclined segment grows steeper while the x distance between two map's extrema vanishes. As s tends to infinity, the Z-map acquires a zig–zag shape with a vertical middle segment. Ringland et $al.$ have shown that in the limiting case $s\to\infty$ the attractors of the Z-map form Farey sequences as other map parameters are varied. They related this property to the existence of a vertical segment since a decrease in s leads to a gradual transformation of Farey sequences into U-sequences. Although the dynamic origin of such maps was not discussed, a possible relation of the Z-map to the existence of mixed-mode oscillations was inferred.

One can easily see that the Z-map in its $s\to\infty$ limit is qualitatively similar to the map $f_Z(x)$ constructed in the present section. In our map the middle segment is always vertical due to the presence of the superunstable orbit. Applying results of Ringland et $al.$ to system (1), we may assume that the repulsive flow defines not only the shape of mixed-mode orbits with their nonoverlapping bands of small- and large-amplitude loops, but also their property to form Farey sequences.

V. CONCLUSIONS

We have analyzed in detail a model exhibiting mixed-mode oscillations. By constructing the model's slow manifold we have shown that mixed-modes correspond to periodic orbits embedded in a horseshoe-type strange set. This explains why chaotic oscillations are observed in transitions between adjacent periodic states. The organization of the slow manifold into a horseshoe also accounts for the signatures of chaos in transient trajectories when the attractor is periodic.

In our model the mixed-mode periodic orbits do not lie on a 2-torus. Following transformations of the slow manifold from its simple planar organization into a horseshoe, we have also shown that a torus does not exist as an intermediate state between period-1 and mixed-mode oscillations. Thus, our scenario for the emergence of mixed-mode oscillations is an alternative to quasiperiodicity.

The main distinctive feature of mixed-mode states, the partition of their orbits into nonoverlapping bands of small- and large-amplitude loops, finds its explanation in the existence of the repulsive flow. Intersection of this flow with the slow manifold yields a complex system of superunstable orbits. The position of the slow manifold relative to the repulsive flow determines whether the formation of small or large loops of the attractor is favored. As parameters change along a path running through the mixed-mode domain, the position of the repulsive flow changes and one observes sequences of mixed-mode states $\mathbf{n}^1\to\mathbf{1}^1\to\mathbf{1}^n(\mathbf{1}^n\to\mathbf{1}^1\to\mathbf{n}^1)$ with monotonously increasing (decreasing) S/L ratio. As the results of Ringland et $al.$[10] suggest, the fact that these sequences are described by Farey arithmetic is also a consequence of the presence of the superunstable orbits. Thus, the existence of the repulsive flow places this horseshoe into a separate subclass of strange sets whose periodic orbits are given by L^S mixed-mode states, and whose windows of periodicity are organized into Farey sequences.

There exist indications that our scenario may account for the mixed-mode oscillations observed in a number of model and experimental studies. This appears to be so for all those cases in which the mixed-mode periodic states were found to be separated by chaotic rather then quasiperiodic oscillations. As Ringland et $al.$[10] pointed out, zig–zag-shaped maps with a vertical middle segment indicative of a superunstable trajectory were found in many chemical and electrochemical systems.

ACKNOWLEDGMENT

[1] J. Maselko and H. L. Swinney, J. Chem. Phys. **85**, 6430 (1986); J. Maselko and H. L. Swinney, Phys. Lett. A **119**, 403 (1987).

[2] R. A. Schmitz, K. R. Graziani, and J. L. Hudson, J. Chem. Phys. **67**, 3040 (1977); J. L. Hudson, M. Hart, and J. Marinko, $ibid.$ **71**, 1601 (1979).

[3] V. Petrov, S. K. Scott, and K. Showalter, J. Chem. Phys. **97**, 6191 (1992); F. Tracqui, Acta Biother. **42**, 147 (1994); for review on mixed-mode

oscillations in chemistry, see I. R. Epstein and K. Showalter, J. Phys. Chem. **100**, 13 132 (1996).

[4] P. Richetti, J. C. Roux, F. Argoul, and A. Arneodo, J. Chem. Phys. **86**, 3339 (1987).

[5] D. Barkley, J. Ringland, and J. S. Turner, J. Chem. Phys. **87**, 3812 (1987).

[6] C. G. Steinmetz and R. Larter, J. Chem. Phys. **94**, 1388 (1991).

[7] F. N. Albahadily, J. Ringland, and M. Schell, J. Chem. Phys. **90**, 813 (1989).

[8] M. T. M. Koper and P. Gaspard, J. Phys. Chem. **95**, 4945 (1991); M. T. M. Koper and P. Gaspard, J. Chem. Phys. **96**, 7797 (1992); M. T. M. Koper, P. Gaspard, and J. H. Sluyters, *ibid.* **97**, 8250 (1992).

[9] M. T. M. Koper, Physica D **80**, 72 (1995).

[10] J. Ringland, N. Issa, and M. Schell, Phys. Rev. A **41**, 4223 (1990).

[11] P. E. Strizhak and A. L. Kawczynski, J. Phys. Chem. **99**, 10 830 (1995).

[12] See Ref. 9 for another possible extension of the Boissonade–De Kepper model.

[13] J. Boissonade and P. J. De Kepper, J. Phys. Chem. **84**, 501 (1980).

[14] Polynomial piece-wise interpolation of the third to fifth order was used in our study. For the particular case considered in this section accurate approximation for the entire Poincaré section is given by the polynomial $z(y) = 0.001y^3 - 0.00432y^2 - 0.22745y + 0.035977$.